Quantum excitation transfer, entanglement, and coherence in a trimer of two-level systems at finite temperature

Ethan Wyke,[*] Abuenameh Aiyejina [ORCID],[†] and Roger Andrews[‡]

Department of Physics, The University of the West Indies, St. Augustine, Trinidad and Tobago

The excitation probabilities, concurrence, and relative entropy of coherence for an array of three coupled two-level systems are studied analytically and numerically at various temperatures. We determine the excitation probabilities for each site, the concurrence between the outer sites, and the relative entropy of coherence of the system for three energy configurations of the trimer and various temperatures. We find that a well configuration (i.e., negative detuning of the inner site) at all temperatures localizes the excitation on the inner site, while a barrier configuration (i.e., positive detuning of the inner site) causes the excitation to be localized on the outer sites. We determine the decay times for the probabilities, concurrence, and relative entropy of coherence for all energy configurations at each temperature. The barrier configuration creates the largest concurrence at zero temperature; however, we find that the uniform configuration is able to resist the loss of quantum coherence and entanglement at higher temperatures more so than any of the other configurations.

I. INTRODUCTION

The phenomenon of quantum coherence has been key to understanding the nonclassical evolution of an excitation in a quantum system. Coherence occurs due to the interference of basis states resulting in the creation of quantum superposition states, which highlights the quantum wave-particle duality that exists at the atomic scale. For a two-level system in a closed quantum environment, near-resonant incident radiation couples the phases of the two levels, creating a coherent quantum system that can truly exist in both states simultaneously. The consequence of this is Rabi oscillations, where populations of the two-level system oscillate as long as this coherence is maintained by the pulse [1]. However, in open quantum systems, superposition states within the Hilbert space display little stability [2], often with decoherence occurring rapidly. Many-body quantum systems compound this issue with the addition of excitation transfer, which can be mediated by interactions such as Heisenberg exchange [3]. This combination of quantum coherence and excitation transfer gives rise to the consideration of entanglement between the components of a many-body system [4].

Liao *et al.* [5] demonstrated the convergence of these three phenomena, i.e., quantum coherence, excitation transfer, and entanglement. They considered a dimer of two-level systems in separate quantum thermal baths, where they simulated coherent excitation transfer probabilities in high- and low-temperature regimes. Pachon and Brumer [6] examined the reasons for long-lived coherence by modeling a photosynthetic dimer in a spin-boson bath. They related the long

decoherence time to the small energy separations, the dimer coupling, and the temperature. Ishizaki and Fleming [7] examined quantum entanglement of a dimer within the light-harvesting complex II in chlorophyllic plants. They found that the steady-state entanglement increased with the monomer coupling and decreased with temperature and reorganization energy.

There has also been research into two-level trimers, which are systems of three coupled two-level quantum systems. Bengtson and Sjoqvist [8] examined the role of quantum coherence in excitation energy transfer between end sites in a trimer without interaction with an environment. They found that while coherence was necessary for population transfer, there was no unique relationship between coherence and the efficiency of the transfer process. Using numerical studies, they calculated the Hamiltonian parameters for optimal time-averaged coherence in the site basis and for optimal population transfer. They found that the parameter values that maximized the time-averaged coherence did not coincide with those that gave perfect population transfer. They also showed that while coherence in the exciton basis matched perfect population transfer in the case of the dimer, this did not occur in the trimer case. Tan and Kuang [9] studied entanglement dynamics and excitation transfer in a light-harvesting complex trimer consisting of two donors and an acceptor interacting with an environment. They showed that there was a quantum phase transition that depended on the detuning between the energies of the different sites. At this phase transition, there was a sudden change in the entanglement between the donors and the acceptor. They found that dissipation lowered the entanglement between the donors, while dephasing enhanced the entanglement for site-energy detunings above a critical value. In another paper, Tan *et al.* [10] investigated a trimer consisting of two acceptors and a donor. They showed that this system also exhibited a quantum phase transition and that in

[*]ethan.wyke@my.uwi.edu
[†]abuenameh.aiyejina@sta.uwi.edu
[‡]roger.andrews@sta.uwi.edu
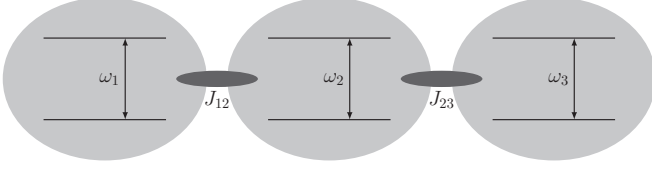
FIG. 1. Schematic of three coupled two-level systems having energy separations ω_1, ω_2, and ω_3, and couplings J_{12} and J_{23}.

the presence of a dephasing environment, there was a sudden change in the probability of excitation transfer from the donor to the acceptors at this phase transition. They found that the dephasing environment could lead to a maximum steady-state transfer probability. Song *et al.* [11] investigated the dynamics of entanglement in a trimer consisting of molecules coupled to environments, with oscillating distances between the molecules. The oscillating distances were manifested as varying coupling strengths between the molecules. They showed that for certain frequencies of oscillation, the entanglement between the first and second molecules could be enhanced at the expense of population transfer. Plenio and Huelga [12], as well as Cao and Silbey [13], showed that in an ordered linear chain, end-to-end excitation transfer could not be assisted by a dephasing environment. Enhanced end-to-end transport occurred only when there was energy detuning. Kassal and Aspuru-Guzik [14] found, using a trimer as an example, that the lack of enhanced transport in an ordered chain was limited to the case of end-to-end transport. They showed that if the initial site for the excitation was the middle site, there was an increase in transport efficiency.

In this paper, we examine a linear array of three coupled two-level systems (trimer) with equal intersite coupling and detuning of the inner site. This system is investigated in the absence of a bath and in the presence of a thermal bath in the perturbative regime with Ohmic spectral density at $T = 0\,\mathrm{K}$, $T = 77\,\mathrm{K}$, and $T = 300\,\mathrm{K}$. In Sec. II, we introduce the general theory of the trimer Hamiltonian, including the system, bath, and system-bath interactions. In Sec. III, we derive analytic expressions for the excitation probabilities of each two-level system, the concurrence between the first and third two-level systems, and the relative entropy of coherence in the absence of the bath and with a thermal bath at $T = 0\,\mathrm{K}$. A numerical approach is then used to solve the Bloch-Redfield master equation for the system in a thermal bath at temperatures 77 and 300 K. Section IV gives results for the excitation probabilities, concurrence, and relative entropy of coherence in the absence of a bath and in a thermal bath at $T = 0\,\mathrm{K}$, $T = 77\,\mathrm{K}$, and $T = 300\,\mathrm{K}$. Finally, the energy configuration that produces the maximum concurrence and maximum relative entropy of coherence is determined for temperatures in the range 0 to 300 K.

II. GENERAL THEORY

In this section, we introduce the theory for three coupled two-level systems (TLSs) coupled to harmonic oscillator baths, with $\hbar = 1$ a.u. (see Fig. 1).

The Hamiltonian of a one-dimensional linear chain of three coupled TLSs is given by

$$H_S = \frac{1}{2}\omega_1\sigma_1^z + \frac{1}{2}\omega_2\sigma_2^z + \frac{1}{2}\omega_3\sigma_3^z + J_{12}(\sigma_1^+\sigma_2^- + \sigma_1^-\sigma_2^+)$$
$$+ J_{23}(\sigma_2^+\sigma_3^- + \sigma_2^-\sigma_3^+), \qquad (1)$$

where ω_i is the energy separation of the ith TLS and $J_{ii'}$ is the dipole-dipole coupling between TLSs i and i'. The TLSs are described by the Pauli operators

$$\sigma_i^+ = (\sigma_i^-)^\dagger = |e\rangle_{ii}\langle g| \qquad (2)$$

and

$$\sigma_i^z = |e\rangle_{ii}\langle e| - |g\rangle_{ii}\langle g|, \qquad (3)$$

where $|g\rangle_i$ and $|e\rangle_i$ are the ground and excited states, respectively, of the ith TLS. The first three terms in Eq. (1) are the free Hamiltonians of the three TLSs and the last two terms describe the dipole-dipole interactions between adjacent TLSs. The state of the system is denoted by $|\alpha\beta\gamma\rangle = |\alpha\rangle_1|\beta\rangle_2|\gamma\rangle_3$, where $\alpha, \beta, \gamma \in \{g, e\}$. The TLSs are coupled to harmonic oscillator baths with the Hamiltonian

$$H_B = H_B^{(a)} + H_B^{(b)} + H_B^{(c)}. \qquad (4)$$

Here, $H_B^{(a)}$, $H_B^{(b)}$, and $H_B^{(c)}$ are the thermal baths for the three TLSs given by

$$H_B^{(a)} = \sum_j \omega_{aj}a_j^\dagger a_j, \quad H_B^{(b)} = \sum_k \omega_{bk}b_k^\dagger b_k,$$
$$H_B^{(c)} = \sum_l \omega_{cl}c_l^\dagger c_l, \qquad (5)$$

where $a_j^\dagger$ (a_j), $b_k^\dagger$ (b_k), and $c_l^\dagger$ (c_l) are the creation (annihilation) operators for the jth, kth, and lth harmonic oscillators with frequencies ω_{aj}, ω_{bk}, and ω_{cl}, respectively. The interaction Hamiltonian of the TLSs with their thermal baths is given by

$$H_I = \sigma_1^+\sigma_1^- \sum_j g_{1j}(a_j^\dagger + a_j) + \sigma_2^+\sigma_2^- \sum_k g_{2k}(b_k^\dagger + b_k)$$
$$+ \sigma_3^+\sigma_3^- \sum_l g_{3l}(c_l^\dagger + c_l), \qquad (6)$$

where g_{1j}, g_{2k}, and g_{3l} are the coupling strengths of the TLSs to their respective thermal baths.

The calculations in this paper use a Bloch-Redfield approach to solve the master equation for the system. The Bloch-Redfield master equation is derived starting from a total Hamiltonian of the form

$$H = H_S + \Delta V + H_B + H_I, \qquad (7)$$

where H_S and H_B are the Hamiltonians of the system and bath, respectively, H_I is the Hamiltonian of the interaction between the system and bath, and ΔV is the counterterm which compensates for the renormalization of the site energies induced by system-bath coupling. The interaction Hamiltonian is decomposed into the general form

$$H_I = \sum_\alpha A_\alpha \otimes B_\alpha, \qquad (8)$$

where the Hermitian operators A_α and B_α act on the system and bath, respectively. For the system considered in this paper, the system and bath operators are given by

$$A_1 = \sigma_1^+ \sigma_1^-, \quad A_2 = \sigma_2^+ \sigma_2^-, \quad A_3 = \sigma_3^+ \sigma_3^- \quad (9)$$

and

$$B_1 = g_{1j}(a_j^\dagger + a_j), \quad B_2 = g_{2k}(b_k^\dagger + b_k),$$
$$B_3 = g_{3l}(c_l^\dagger + c_l). \quad (10)$$

We assume that each site is coupled to separate baths with identical properties, and therefore, we disregard the counterterm in Eq. (7). We can define the operators

$$A_\alpha(\omega) = \sum_{\varepsilon' - \varepsilon = \omega} \Pi(\varepsilon) A_\alpha \Pi(\varepsilon'), \quad (11)$$

where $\Pi(\varepsilon)$ is the projector onto the eigenspace belonging to the eigenvalue ε of H_S and the sum extends over all energy eigenvalues ε' and ε of H_S with a fixed energy difference of ω. In addition, the influence of the bath on the system can be described by a spectral function. The spectral function is the Fourier transform of the bath correlation functions and is defined by

$$S_{\alpha\beta}(\omega) = \int_{-\infty}^{\infty} e^{i\omega\tau} \langle B_\alpha(\tau) B_\beta(0)\rangle d\tau. \quad (12)$$

The Bloch-Redfield master equation without the secular approximation is then given by [2]

$$\frac{d}{dt}\rho_S(t) = -i[H_S, \rho_S(t)] + \sum_{\omega,\omega'} \sum_{\alpha,\beta} \sqrt{S_{\alpha\beta}(\omega)S_{\alpha\beta}(\omega')}$$
$$\times [A_\beta(\omega)\rho_S(t)A_\alpha^\dagger(\omega')$$
$$- A_\alpha^\dagger(\omega')A_\beta(\omega)\rho_S(t) + \text{H.c.}], \quad (13)$$

where ρ_S is the density matrix of the system.

For the simulations in this paper, we use harmonic oscillator baths with an Ohmic spectral density that is given by

$$\mathcal{J}(\omega) = \kappa\omega, \quad (14)$$

where κ controls the strength of the coupling between the TLSs and their baths. The Bloch-Redfield equation is valid only in the weak-coupling regime, which is defined by the condition $\eta \ll 1$, where $\eta = \frac{2\kappa}{\pi^2}$ [15]. Assuming that the bath for the ith TLS is in thermal equilibrium at temperature T_i and that cross-correlations vanish, the Fourier transforms of the bath correlation functions are given by

$$S_i(\omega) = \begin{cases} 2\kappa \frac{k_B T_i}{\hbar} & \text{if } \omega = 0, \\ \mathcal{J}(\omega)\exp\left(\frac{\hbar\omega}{k_B T_i}\right)\coth\left(\frac{\hbar\omega}{2k_B T_i}\right) & \text{if } \omega < 0, \\ \mathcal{J}(\omega)\coth\left(\frac{\hbar\omega}{2k_B T_i}\right) & \text{if } \omega > 0, \end{cases} \quad (15)$$

where k_B is Boltzmann's constant.

We evaluate the excitation probabilities of the three TLSs during the evolution of the system. These probabilities are obtained from the reduced density matrix of each TLS. The reduced density matrix of the ith TLS is given by

$$\rho_i = \text{Tr}_{jk}[\rho_S], \quad (16)$$
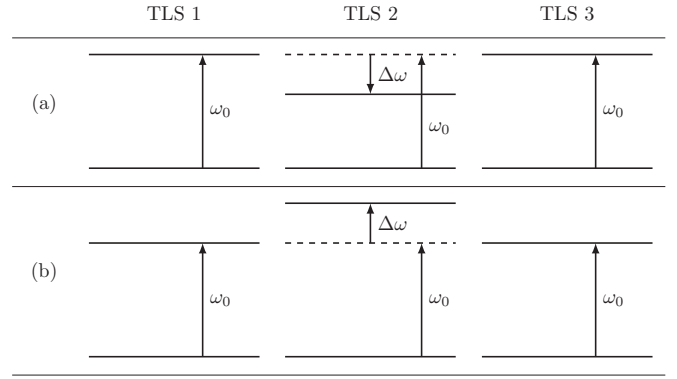
FIG. 2. Schematics of two energy separation configurations for (a) a well with $\Delta\omega > 0$ and (b) a barrier with $\Delta\omega < 0$.

where ρ_S is the density matrix of the system and the remaining jth and kth TLSs have been traced out. The excitation probability of the ith TLS is then given by

$$P_i(t) = \text{Tr}[\rho_i \sigma_i^+ \sigma_i^-]. \quad (17)$$

We also study the quantum entanglement between the TLSs using the concurrence. In order to calculate the concurrence between the ith and jth TLSs, the reduced density matrix of the subsystem consisting of the ith and jth TLSs is used. This density matrix is given by

$$\rho_{ij} = \text{Tr}_k[\rho_S], \quad (18)$$

where the remaining kth TLS has been traced out. The concurrence of this density matrix is given by

$$C_{ij} = C(\rho_{ij}) = \max\{0, \sqrt{s_1} - \sqrt{s_2} - \sqrt{s_3} - \sqrt{s_4}\}, \quad (19)$$

where $s_n(n = 1, 2, 3, 4)$ are the eigenvalues of the matrix $\rho_{ij}\tilde{\rho}_{ij}$ such that $s_1 \geqslant s_2 \geqslant s_3 \geqslant s_4$. The operator $\tilde{\rho}_{ij}$ is the spin-flipped density matrix defined as

$$\tilde{\rho}_{ij} = \left(\sigma_i^y \otimes \sigma_j^y\right)\rho_{ij}^*\left(\sigma_i^y \otimes \sigma_j^y\right), \quad (20)$$

where ρ_{ij}^* is the complex conjugate of ρ_{ij} and σ_i^y is the Pauli matrix in the y direction for the ith TLS [16].

Finally, we investigate the evolution of the coherence of the system using the relative entropy of coherence as a measure. The relative entropy of coherence of the system is given by

$$C_{\text{rel.ent.}}(\rho_S) = S(\rho_{S,\text{diag}}) - S(\rho_S), \quad (21)$$

where $\rho_{S,\text{diag}}$ is the density matrix obtained from ρ_S by setting all off-diagonal elements to zero and

$$S(\rho) = -\text{Tr}[\rho \ln \rho] \quad (22)$$

is the von Neumann entropy of the density matrix ρ [17].

III. THEORY OF A TRIMER

Using ω_0 and $\Delta\omega$ as seen in Fig. 2, the energies, $\omega_1, \omega_2,$ and ω_3, can be expressed as

$$\omega_1 = \omega_3 = \omega_0, \quad \omega_2 = \omega_0 - \Delta\omega, \quad (23)$$

where $\Delta\omega = \omega_0 - \omega_2$ is the detuning. The mixing angle θ is defined by

$$\tan\theta = \frac{2\sqrt{2}J}{\Delta\omega} \tag{24}$$

and follows a definition similar to that used by Liao *et al.* [5]. When $\theta = 0.5\pi$, we have $\Delta\omega = 0$ and $\omega_1 = \omega_2 = \omega_3$, which correspond to the uniform configuration. As seen in Fig. 2(a), when $\theta < 0.5\pi$, we have $\Delta\omega > 0$ and $\omega_2 < \omega_1 = \omega_3$, which correspond to the well configuration. When $\theta > 0.5\pi$, we have $\Delta\omega < 0$ and $\omega_2 > \omega_1 = \omega_3$, which correspond to the barrier configuration, as seen in Fig. 2(b).

A. Trimer with no bath

We assume equal dipole-dipole couplings such that $J_{12} = J_{23} = J$. In this case, the Hamiltonian of the trimer becomes

$$H_S = \frac{1}{2}\omega_0\sigma_1^z + \frac{1}{2}(\omega_0 - \Delta\omega)\sigma_2^z + \frac{1}{2}\omega_0\sigma_3^z$$
$$+ J(\sigma_1^+\sigma_2^- + \sigma_1^-\sigma_2^+ + \sigma_2^+\sigma_3^- + \sigma_2^-\sigma_3^+). \tag{25}$$

Using the initial state $|\Psi(0)\rangle = |egg\rangle$, the wave function for the system at time t, $|\Psi(t)\rangle$, can be found from

$$|\Psi(t)\rangle = e^{-iH_S t}|\Psi(0)\rangle, \tag{26}$$

where H_S is diagonal in the basis defined in Eqs. (A1a)–(A1f) in Appendix A. From the density matrix, $\rho_S = |\Psi(t)\rangle\langle\Psi(t)|$, the excitation probabilities as functions of time are determined to be

$$P_1(t) = \frac{1}{4}\{[\cos(\sqrt{2}Jt\cot\theta) + \cos(\sqrt{2}Jt\csc\theta)]^2$$
$$+ [\sin(\sqrt{2}Jt\cot\theta) + \cos\theta\sin(\sqrt{2}Jt\csc\theta)]^2\}, \tag{27a}$$

$$P_2(t) = \frac{1}{2}\sin^2\theta\sin^2(\sqrt{2}Jt\csc\theta), \tag{27b}$$

$$P_3(t) = \frac{1}{4}\{[\cos(\sqrt{2}Jt\cot\theta) - \cos(\sqrt{2}Jt\csc\theta)]^2$$
$$+ [\sin(\sqrt{2}Jt\cot\theta) - \cos\theta\sin(\sqrt{2}Jt\csc\theta)]^2\}. \tag{27c}$$

In the ordered basis $\{|ee\rangle, |eg\rangle, |ge\rangle, |gg\rangle\}$, an "$X$"-class state has the density matrix

$$\rho = \begin{pmatrix} \sigma_{11} & 0 & 0 & \sigma_{14} \\ 0 & \sigma_{22} & \sigma_{23} & 0 \\ 0 & \sigma_{32} & \sigma_{33} & 0 \\ \sigma_{41} & 0 & 0 & \sigma_{44} \end{pmatrix}, \tag{28}$$

where $\sigma_{23} = \sigma_{32}^*$ and $\sigma_{14} = \sigma_{41}^*$ as ρ is Hermitian. When Eq. (19) is applied to ρ, it simplifies to [18]

$$C(\rho) = \max\{0, 2(|\sigma_{23}| - \sqrt{\sigma_{11}\sigma_{44}}), 2(|\sigma_{14}| - \sqrt{\sigma_{22}\sigma_{33}})\}. \tag{29}$$

The expression $\sqrt{s_1} - \sqrt{s_2} - \sqrt{s_3} - \sqrt{s_4}$ in Eq. (19), when applied to $\rho\tilde{\rho}$, gives two expressions whose values can be greater than zero, and these are incorporated into Eq. (29). Using Eq. (18), the reduced density matrix of the first and third TLSs ρ_{13} is found to have the form

$$\rho_{13} = \begin{pmatrix} 0 & 0 & 0 & 0 \\ 0 & \sigma_{22} & \sigma_{23} & 0 \\ 0 & \sigma_{32} & \sigma_{33} & 0 \\ 0 & 0 & 0 & \sigma_{44} \end{pmatrix} \tag{30}$$

in the ordered basis $\{|ee\rangle, |eg\rangle, |ge\rangle, |gg\rangle\}$. Since $\sigma_{11} = \sigma_{14} = 0$ in this instance, the concurrence of this density matrix simplifies to

$$C_{13} = C(\rho_{13}) = 2|\sigma_{23}|. \tag{31}$$

Using the solution for ρ_{13} in Eq. (30), we can obtain σ_{23}, and hence, the concurrence is given as

$$C_{13} = \left| \frac{1}{2}\{\cos(\sqrt{2}Jt\cot\theta) + \cos(\sqrt{2}Jt\csc\theta)\right.$$
$$+ i[\sin(\sqrt{2}Jt\cot\theta) + \cos\theta\sin(\sqrt{2}Jt\csc\theta)]\}$$
$$\times \{\cos(\sqrt{2}Jt\cot\theta) - \cos(\sqrt{2}Jt\csc\theta)$$
$$\left. - i[\sin(\sqrt{2}Jt\cot\theta) - \cos\theta\sin(\sqrt{2}Jt\csc\theta)]\} \right|. \tag{32}$$

From Eqs. (27) and (32), it can be seen that the excitation probability of the second TLS P_2 oscillates at a frequency of $\omega_P = 2\sqrt{2}J\csc\theta$, while the excitation probabilities of the first and third TLSs (P_1 and P_3), as well as the concurrence C_{13}, exhibit oscillations at three frequencies: $\omega_P = 2\sqrt{2}J\csc\theta$, $\omega_P' = \sqrt{2}J\tan\frac{\theta}{2}$, and $\omega_P'' = \sqrt{2}J\cot\frac{\theta}{2}$. The relative entropy of coherence is found using Eq. (21) and is determined to be

$$C_{\text{rel.ent.}} = -\frac{1}{2}\ln\left[\frac{1}{2}\sin^2\theta\sin^2(\sqrt{2}Jt\csc\theta)\right]\sin^2\theta\sin^2(\sqrt{2}Jt\csc\theta) - \frac{1}{4}\ln\left(\frac{1}{4}\{[\cos(\sqrt{2}Jt\cot\theta) - \cos(\sqrt{2}Jt\csc\theta)]^2\right.$$
$$+ [\sin(\sqrt{2}Jt\cot\theta) - \cos\theta\sin(\sqrt{2}Jt\csc\theta)]^2\}) \times \{[\cos(\sqrt{2}Jt\cot\theta) - \cos(\sqrt{2}Jt\csc\theta)]^2$$
$$+ [\sin(\sqrt{2}Jt\cot\theta) - \cos\theta\sin(\sqrt{2}Jt\csc\theta)]^2\} - \frac{1}{4}\ln\left(\frac{1}{4}\{[\cos(\sqrt{2}Jt\cot\theta) + \cos(\sqrt{2}Jt\csc\theta)]^2\right.$$
$$+ [\sin(\sqrt{2}Jt\cot\theta) + \cos\theta\sin(\sqrt{2}Jt\csc\theta)]^2\}) \times \{[\cos(\sqrt{2}Jt\cot\theta) + \cos(\sqrt{2}Jt\csc\theta)]^2$$
$$+ [\sin(\sqrt{2}Jt\cot\theta) + \cos\theta\sin(\sqrt{2}Jt\csc\theta)]^2\}. \tag{33}$$

B. Trimer in a bath at absolute zero

In the limit of zero temperature, the spectral function becomes

$$S_{T\to 0}(\omega) = \begin{cases} 0, & \omega < 0, \\ \kappa\omega, & \omega \geqslant 0, \end{cases} \tag{34}$$

where κ controls the strength of the coupling between the TLSs and their baths. Using Eqs. (25) and (34) to solve Eq. (13), with the initial state $|egg\rangle$, gives the solution for the density matrix in the zero-temperature limit $\rho_{S,T\to0}$. The reduced density matrix for the ith TLS in the zero-temperature limit is given by

$$\rho_{i,T\to0} = \text{Tr}_{jk}[\rho_{S,T\to0}]. \tag{35}$$

The excitation probability of the ith TLS is then given by

$$P_{i,T\to0}(t) = \text{Tr}[\rho_{i,T\to0}\sigma_i^+\sigma_i^-]. \tag{36}$$

Calculating the excitation probabilities using Eq. (36) gives the following:

$$
\begin{aligned}
P_{1,T\to0}(t) = {}& \frac{1}{2}\sin^2\left(\frac{\theta}{2}\right) + \frac{1}{24}(\cos\theta + 7)\cos^2\left(\frac{\theta}{2}\right)\exp\left(-\frac{1}{2\sqrt{2}}\kappa Jt\sin\theta\right) \\
& + \frac{1}{24}(5\cos\theta - 1)\cos^2\left(\frac{\theta}{2}\right)\exp(-\sqrt{2}\kappa Jt\sin\theta) \\
& + \frac{1}{8}\sin^2\theta\cos(2\sqrt{2}Jt\csc\theta)\exp\left(-\frac{1}{\sqrt{2}}\kappa Jt\sin\theta\right) \\
& + \frac{1}{2}\sin^2\left(\frac{\theta}{2}\right)\cos\left(\sqrt{2}Jt\cot\frac{\theta}{2}\right)\exp\left(-\frac{1}{4\sqrt{2}}\kappa Jt\sin\theta\right) \\
& + \frac{1}{2}\cos^2\left(\frac{\theta}{2}\right)\cos\left(\sqrt{2}Jt\tan\frac{\theta}{2}\right)\exp\left(-\frac{5}{4\sqrt{2}}\kappa Jt\sin\theta\right) + C,
\end{aligned}
\tag{37a}
$$

$$
\begin{aligned}
P_{2,T\to0}(t) = {}& \cos^2\left(\frac{\theta}{2}\right) - \frac{1}{12}\cos^2\left(\frac{\theta}{2}\right)(\cos\theta + 7)\exp\left(-\frac{1}{2\sqrt{2}}\kappa Jt\sin\theta\right) \\
& - \frac{1}{12}\cos^2\left(\frac{\theta}{2}\right)(5\cos\theta - 1)\exp(-\sqrt{2}\kappa Jt\sin\theta) \\
& - \frac{1}{4}\sin^2\theta\cos(2\sqrt{2}Jt\csc\theta)\exp\left(-\frac{1}{\sqrt{2}}\kappa Jt\sin\theta\right),
\end{aligned}
\tag{37b}
$$

$$
\begin{aligned}
P_{3,T\to0}(t) = {}& \frac{1}{2}\sin^2\left(\frac{\theta}{2}\right) + \frac{1}{24}(\cos\theta + 7)\cos^2\left(\frac{\theta}{2}\right)\exp\left(-\frac{1}{2\sqrt{2}}\kappa Jt\sin\theta\right) \\
& + \frac{1}{24}(5\cos\theta - 1)\cos^2\left(\frac{\theta}{2}\right)\exp(-\sqrt{2}\kappa Jt\sin\theta) \\
& + \frac{1}{8}\sin^2\theta\cos(2\sqrt{2}Jt\csc\theta)\exp\left(-\frac{1}{\sqrt{2}}\kappa Jt\sin\theta\right) \\
& - \frac{1}{2}\sin^2\left(\frac{\theta}{2}\right)\cos\left(\sqrt{2}Jt\cot\frac{\theta}{2}\right)\exp\left(-\frac{1}{4\sqrt{2}}\kappa Jt\sin\theta\right) \\
& - \frac{1}{2}\cos^2\left(\frac{\theta}{2}\right)\cos\left(\sqrt{2}Jt\tan\frac{\theta}{2}\right)\exp\left(-\frac{5}{4\sqrt{2}}\kappa Jt\sin\theta\right) - C,
\end{aligned}
\tag{37c}
$$

where

$$
\begin{aligned}
C = {}& \frac{\kappa\sin\theta}{8\sqrt{\kappa^2 + 16\cot^2\theta\csc^2\theta}}\left[\cos\left(\sqrt{2}Jt\cot\frac{\theta}{2} - \varphi\right)\exp\left(-\frac{1}{4\sqrt{2}}\kappa Jt\sin\theta\right)\right. \\
& \left. - \cos\left(\sqrt{2}Jt\tan\frac{\theta}{2} - \varphi\right)\exp\left(-\frac{5}{4\sqrt{2}}\kappa Jt\sin\theta\right)\right]
\end{aligned}
\tag{38}
$$

and

$$\varphi = \tan^{-1}\left(\frac{4\cot\theta\csc\theta}{\kappa}\right). \tag{39}$$

The reduced density matrix of the first and third TLSs in the zero-temperature limit $\rho_{13,T\to 0}(t)$ is substituted into Eq. (31) to give the following concurrence $C_{13,T\to 0}$:

$$
\begin{aligned}
C_{13,T\to 0} = \Bigg| & \sin^2\left(\frac{\theta}{2}\right) + \frac{1}{12}\left[\cos^2\left(\frac{\theta}{2}\right) - 2\right](\cos\theta + 7)\exp\left(-\frac{1}{2\sqrt{2}}\kappa Jt\sin\theta\right) \\
& + \frac{1}{12}(5\cos\theta + 3)\cos^2\left(\frac{\theta}{2}\right)\exp(-\sqrt{2}\kappa Jt\sin\theta) \\
& + \frac{1}{4}\sin^2\theta\cos(2\sqrt{2}Jt\csc\theta)\exp\left(-\frac{1}{\sqrt{2}}\kappa Jt\sin\theta\right) \\
& + i\Bigg\{\sin^2\left(\frac{\theta}{2}\right)\sin\left(\sqrt{2}Jt\cot\frac{\theta}{2}\right)\exp\left(-\frac{1}{4\sqrt{2}}\kappa Jt\sin\theta\right) \\
& - \cos^2\left(\frac{\theta}{2}\right)\sin\left(\sqrt{2}Jt\tan\frac{\theta}{2}\right)\exp\left(-\frac{5}{4\sqrt{2}}\kappa Jt\sin\theta\right) \\
& + \frac{\kappa\sin\theta}{4\sqrt{\kappa^2 + 16\cot^2\theta\csc^2\theta}}\Bigg[\sin\left(\sqrt{2}Jt\cot\frac{\theta}{2} - \varphi\right)\exp\left(-\frac{1}{4\sqrt{2}}\kappa Jt\sin\theta\right) \\
& - \sin\left(\sqrt{2}Jt\tan\frac{\theta}{2} - \varphi\right)\exp\left(-\frac{5}{4\sqrt{2}}\kappa Jt\sin\theta\right)\Bigg]\Bigg\}\Bigg|.
\end{aligned}
\tag{40}
$$

Using the density matrix $\rho_{S,T\to 0}(t)$ in Eq. (21), an analytical solution is found (but not stated in the paper due to its length) for the relative entropy of coherence in the zero-temperature limit $C_{\text{rel.ent.},T\to 0}$, which is plotted in Sec. IV.

C. Trimer in a bath at nonzero temperature

A numerical approach is used to solve the Bloch-Redfield master equation [see Eq. (13)] for a thermal bath. This approach is used to generate solutions for two bath temperatures, $T = 77\,\text{K}$ and $T = 300\,\text{K}$. For each temperature, in addition to calculating the excitation probabilities for each TLS, two other time-dependent quantities are calculated: the concurrence between the first and third TLSs C_{13} [see Eq. (19)] and the relative entropy of coherence of the system $C_{\text{rel.ent.}}$ [see Eq. (21)]. It is found that the numerical solutions of P_1, P_2, and P_3 at $T = 77\,\text{K}$ and $T = 300\,\text{K}$ exhibit similarities to the solutions for P_1, P_2, and P_3 at $T = 0\,\text{K}$. The function $F_1(t)$ is found to be a good approximation for the nonzero temperature probabilities,

$$
F_1(t) = \alpha_1 e^{-\gamma_1 t} + \beta_1 e^{-\lambda_1 t}\sin(\Omega_1 t) + F_{1,\text{asym}},
\tag{41}
$$

where $F_{1,\text{asym}}$ is the asymptotic value of $F_1(t)$, λ_1 and γ_1 are decay constants, with λ_1 determining the rate of decay of the oscillations, and Ω_1 is the angular frequency of the damped oscillations. It should be noted that α_1, β_1, γ_1, λ_1, Ω_1, and $F_{1,\text{asym}}$ depend on the temperature T, the mixing angle θ, and the system-bath coupling strength κ. Specifically, the decay constants γ_1 and λ_1 (which determine the decay rates) both increase with κ and T. It is found that increasing either κ or T tends to increase the value of $S(\omega)$ at the eigenenergy gap. This increase in $S(\omega)$ at the eigenenergy gap results in an increase in the decay rates. F_1 was used as a best-fit curve to the numerical results for the nonzero temperature probabilities obtained using the Bloch-Redfield equation. The best-fit curve can then be easily used to obtain the values of the frequency of

the oscillations Ω_1, the decay times, and the asymptotic values of the probabilities.

Similarly, the function $F_2(t)$ is found to be a good approximation for the concurrence and relative entropy of coherence,

$$
\begin{aligned}
F_2(t) = \big| & \alpha_2 e^{-\gamma_2 t} + \beta_2 e^{-\lambda_2 t}\cos(\Omega_2 t) + i[\alpha' e^{-\lambda_2' t}\sin(\Omega_2' t) \\
& + \beta' e^{-\lambda_2'' t}\sin(\Omega_2'' t)] + F_{2,\text{asym}}\big|,
\end{aligned}
\tag{42}
$$

where Ω_2, Ω_2', and Ω_2'' are the angular frequencies. Furthermore, γ_2, λ_2, λ_2', and λ_2'' are decay constants, while $F_{2,\text{asym}}$ is the asymptotic value of $F_2(t)$. Also, similar to the parameters in Eq. (41), each parameter in Eq. (42) depends on the temperature T, the mixing angle θ, and the system-bath coupling strength κ. Similar to what was found for F_1, the decay constants λ_2 and γ_2 both increase as either κ or T increases. An increase in $S(\omega)$ at the eigenenergy gap also leads to an increase in the decay rates. F_2 was used as a best-fit curve to the numerical results for the nonzero temperature concurrences and relative entropies of coherence obtained using the density matrices from the Bloch-Redfield equation. The best-fit curve can then be easily used to obtain the values of the frequency of the oscillations (either Ω_2, Ω_2', or Ω_2''), the decay times, and the asymptotic values of the concurrences and relative entropies of coherence.

IV. RESULTS

A. Excitation probabilities for a trimer with no bath and with a thermal bath at absolute zero

Figure 3 shows plots of the analytically derived solutions for P_1, P_2, and P_3 given in Eq. (27), with $\kappa = 0$, $J = 87.7\,\text{cm}^{-1}$, and $\omega_0 = 12\,000\,\text{cm}^{-1}$. These equations describe the excitation probabilities of the trimer in the absence of a thermal bath for an initial state $|egg\rangle$. Figure 3 also shows the corresponding plots for P_1, P_2, and P_3 for a trimer in a zero-temperature bath, as given in Eq. (37), with $\kappa = 0.1$,
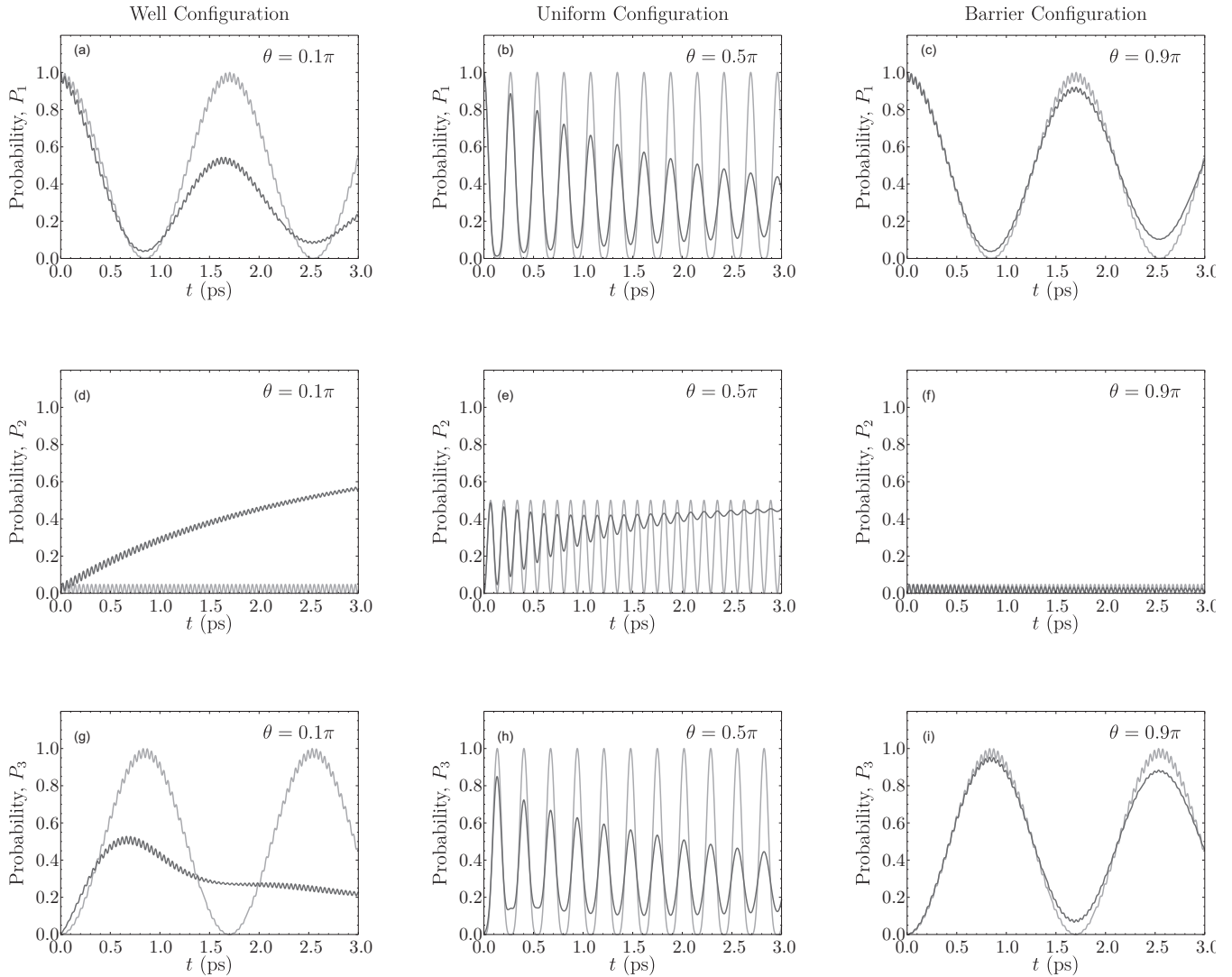
FIG. 3. Plots of the analytic results for the excitation probabilities (a)–(c) P_1, (d)–(f) P_2, and (g)–(i) P_3 for $\theta = 0.1\pi, 0.5\pi, 0.9\pi$ in the absence of a bath (light gray line) and in the presence of a zero-temperature bath (dark gray line).

$J = 87.7\,\mathrm{cm}^{-1}$, and $\omega_0 = 12\,000\,\mathrm{cm}^{-1}$. The value of $\kappa = 0.1$ is suitable for the weak-coupling regime since $\eta = 0.02 \ll 1$.

From Fig. 3, it is observed that P_1, P_2, and P_3 are identical for the well ($\theta = 0.1\pi$, $|\Delta\omega| = 763.4\,\mathrm{cm}^{-1}$) and barrier ($\theta = 0.9\pi$, $|\Delta\omega| = 763.4\,\mathrm{cm}^{-1}$) configurations in the absence of a bath. It should be noted that $\theta = 0.1\pi$ and $\theta = 0.9\pi$ give a well depth and barrier height of the same magnitude. P_1 and P_3 oscillate between 0 and 1 with a frequency of 0.59 THz (and a phase difference of π), and P_2 oscillates between 0 and 0.05 with a frequency of 24.1 THz. For the uniform configuration ($\theta = 0.5\pi$, $|\Delta\omega| = 0\,\mathrm{cm}^{-1}$), also in the absence of a bath, P_1 and P_3 oscillate between 0 and 1 at 3.72 THz (with a phase difference of π), and P_2 oscillates between 0 and 0.5 at 7.43 THz. It is therefore observed that the well and barrier configurations reduce the oscillation frequency of P_1 and P_3 compared to that of the uniform configuration. However, the well and barrier configurations reduce the amplitude of the oscillations of P_2 significantly, with the oscillation frequency of P_2 being smaller for the uniform configuration compared to the well and barrier configurations. Hence, the well and

barrier configurations suppress the amplitude of P_2, as well as the oscillation frequency of P_1 and P_3.

For the trimer in the presence of a bath at $T = 0\,\mathrm{K}$ (with $\kappa = 0.1$), P_1, P_2, and P_3 all display different temporal profiles for the well configuration, barrier configuration, and uniform configuration, as seen in Fig. 3. For the well configuration, P_1 and P_3 exhibit damped oscillations with a frequency of 0.59 THz (and a phase difference of π), which decay to 1% of their initial amplitude in 13 ps and reach an asymptotic value of 0.01 in 44 ps. P_2 increases steadily from zero towards an asymptotic value of 0.98 in 23 ps. As P_2 increases, it exhibits small-amplitude decaying oscillations with a frequency of 24.1 THz. In the barrier configuration, P_1 and P_3 exhibit damped oscillations with a frequency of 0.59 THz (and a phase difference of π), which decay to 1% of their initial amplitude in 51 ps, approaching an asymptotic value of 0.49. P_2 for the barrier exhibits oscillations of negligible amplitude with a frequency of 24.1 THz. For the uniform configuration, P_1 and P_3 exhibit damped oscillations with a frequency of 3.72 THz (and a phase difference of π), which decay to 1%
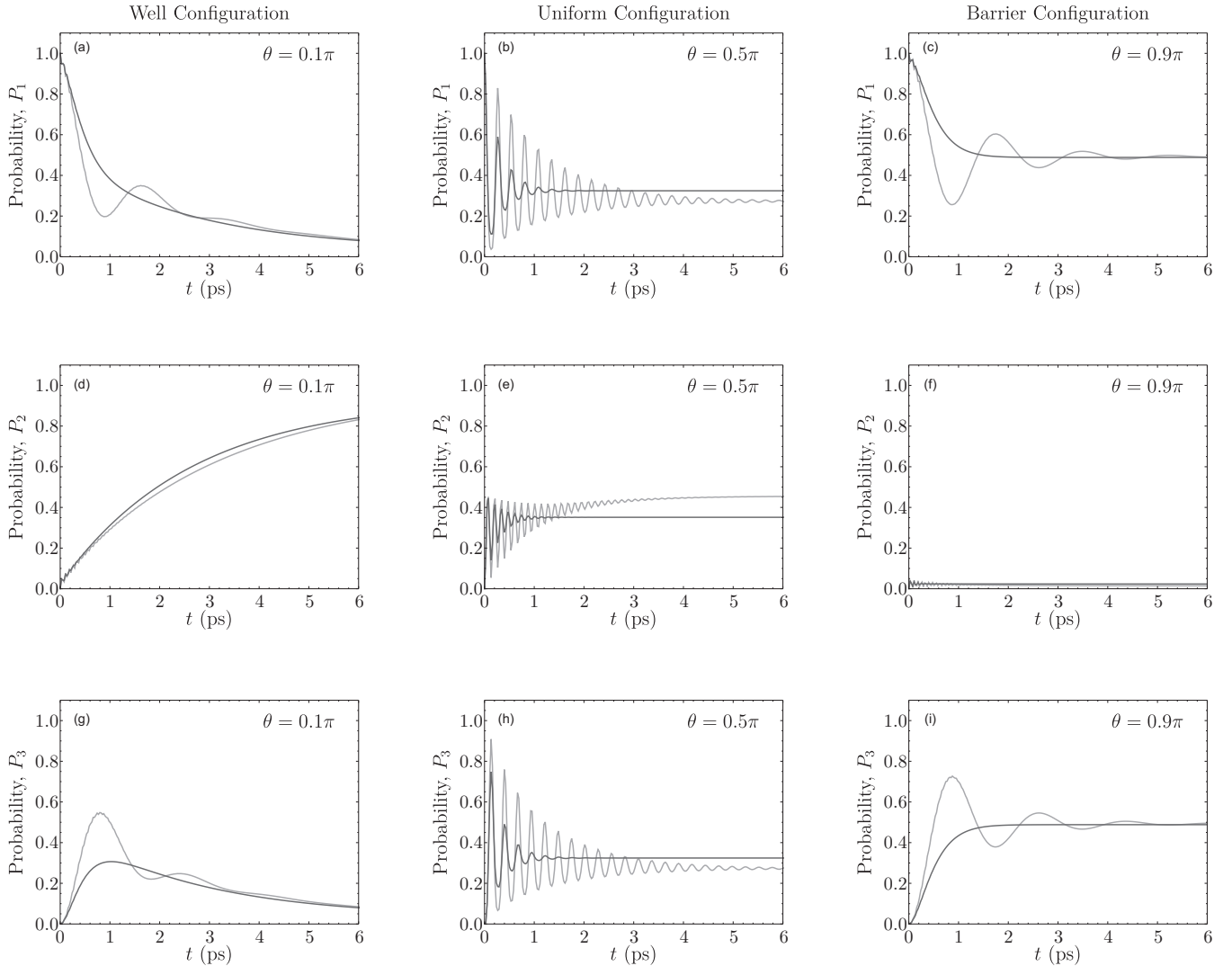
FIG. 4. Plots of the numerical results for the excitation probabilities (a)–(c) P_1, (d)–(f) P_2, and (g)–(i) P_3 for $\theta = 0.1\pi, 0.5\pi, 0.9\pi$ with bath temperatures of $T = 77$ K (light gray line) and $T = 300$ K (dark gray line).

of their initial amplitude in 15 ps, approaching an asymptotic value of 0.25 in 7 ps. P_2 exhibits damped oscillations with a frequency of 7.44 THz, with a steady increase in the values of the minima, and reaches an asymptotic value of 0.5 in 7 ps.

B. Excitation probabilities for a trimer in a thermal bath at $T = 77$ K and $T = 300$ K

Figure 4 shows plots of the numerically derived solutions for P_1, P_2, and P_3 in the presence of a bath at temperatures $T = 77$ K and $T = 300$ K. The simulations were done using two approaches: a PYTHON-based code employing the QUTIP package's Bloch-Redfield master-equation solver [19] and a *Mathematica* program written by the authors for numerical integration of the Bloch-Redfield equation. Both approaches yielded the same results. The results are shown for $\kappa = 0.1$, $J = 87.7$ cm^{-1}, and $\omega_0 = 12\,000$ cm^{-1}.

In the well configuration, P_1 and P_3 exhibit damped oscillations with a frequency of 0.52 THz (and a phase difference of π) at 77 K, while at 300 K, damping with no appreciable oscillations is observed. At 77 K, the

oscillations decay to 1% of their initial amplitude in 3.9 ps and reach an asymptotic value of 0.01 in 26 ps. The details of this calculation are given in Sec. B 1. At 300 K, P_1 decreases exponentially from 1 to an asymptotic value of 0.03 in 19 ps, and P_3 increases from zero to a maximum and then decreases to an asymptotic value of 0.03 in 19 ps. P_2 increases steadily from zero to an asymptotic value of 0.98 in 14 ps at 77 K and 0.93 in 12 ps at 300 K. At 77 K, P_2 exhibits small-amplitude, high-frequency oscillations with a frequency of 13.6 THz, while at 300 K, damping with no appreciable oscillations is observed.

For the barrier configuration, P_1 and P_3 exhibit damped oscillations with a frequency of 0.55 THz (and a phase difference of π) at 77 K, while at 300 K, damping with no appreciable oscillations is observed. At 77 K, the oscillations decay to 1% of their initial amplitude in 5.8 ps and reach an asymptotic value of 0.49. At 300 K, P_1 decreases exponentially from 1 to an asymptotic value of 0.49 in 2.9 ps, while P_3 increases from zero to an asymptotic value of 0.49 in 2.9 ps. P_2 exhibits oscillations of negligible amplitude
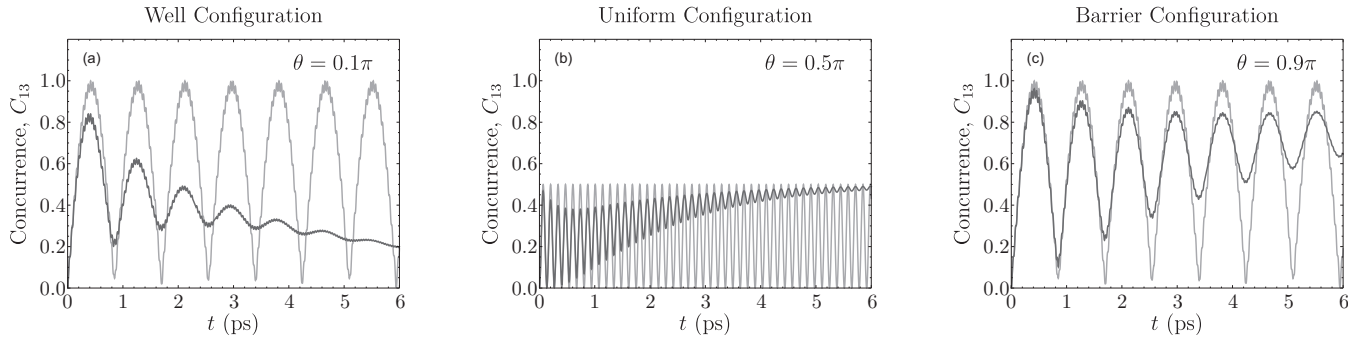
FIG. 5. Plots of the analytic results for the concurrence C_{13} for $\theta = 0.1\pi, 0.5\pi, 0.9\pi$ in the absence of a bath (light gray line) and in the presence of a zero-temperature bath (dark gray line).

with a frequency of 13.6 THz at 77 K and of 13.7 THz at 300 K.

For the uniform configuration, P_1 and P_3 exhibit damped oscillations with a frequency of 3.7 THz at 77 K and of 3.63 THz at 300 K (and a phase difference of π). At 77 K, the oscillations decay to 1% of their initial amplitude in 5.5 ps and reach an asymptotic value of 0.27 in 4.8 ps. At 300 K, the oscillations decay to 1% of their initial amplitude in 1.5 ps, reaching an asymptotic value of 0.32. P_2 exhibits damped oscillations with a frequency of 7.43 THz at 77 K and of 7.35 THz at 300 K. At 77 K, P_2 displays a steady increase in the values of the minima and reaches an asymptotic value of 0.46 in 5.1 ps. At 300 K, P_2 displays a steady increase in the values of the minima and reaches an asymptotic value of 0.35 in 1.3 ps.

C. Concurrence for a trimer with no bath and with a thermal bath at absolute zero

Figure 5 shows plots of the analytically derived solution for C_{13} given in Eq. (32), with $\kappa = 0$, $J = 87.7 \, \text{cm}^{-1}$, and $\omega_0 = 12\,000 \, \text{cm}^{-1}$ for an initial state $|egg\rangle$. Figure 5 also shows the corresponding plots for C_{13} for a trimer in a zero-temperature bath, as given in Eq. (40), with $\kappa = 0.1$, $J = 87.7 \, \text{cm}^{-1}$, and $\omega_0 = 12\,000 \, \text{cm}^{-1}$.

From Fig. 5, it is observed that C_{13} is identical for the well and barrier configurations in the absence of a bath, oscillating between 0 and 1 with a frequency of 0.59 THz. For the uniform configuration, C_{13} oscillates between 0 and 0.5 with a frequency of 7.43 THz. It is therefore observed that the well

and barrier configurations reduce the oscillation frequency of C_{13} compared to that of the uniform configuration. However, the well and barrier configurations enhance the amplitude of the oscillations of C_{13} significantly.

For the trimer in the presence of a bath at $T = 0$ K (with $\kappa = 0.1$), C_{13} displays different temporal profiles for the well and barrier configurations, as seen in Fig. 5. For the well configuration, C_{13} exhibits damped oscillations with a frequency of 0.59 THz, goes to zero in 18.4 ps, and then approaches an asymptotic value of 0.02 at 22.2 ps. In the barrier configuration, C_{13} exhibits damped oscillations with a frequency of 0.59 THz, with a steady increase in the values of the minima, and approaches an asymptotic value of 0.98 in 26 ps. For the uniform configuration, C_{13} exhibits damped oscillations with a frequency of 3.72 THz, with a steady increase in the values of the minima, and approaches an asymptotic value of 0.5 in 9 ps.

D. Concurrence for a trimer in a thermal bath at $T = 77$ K and $T = 300$ K

Figure 6 shows plots of the numerically derived solutions for C_{13} in the presence of the bath at temperatures $T = 77$ K and $T = 300$ K. The results are shown for $\kappa = 0.1$, $J = 87.7 \, \text{cm}^{-1}$, and $\omega_0 = 12\,000 \, \text{cm}^{-1}$, using the same numerical methods as in Sec. IV B.

In the well configuration, C_{13} consists of damped oscillations with a frequency of 0.57 THz at 77 K, while at 300 K, damping with no appreciable oscillations is observed. At 77 K, C_{13} goes to zero in 8.1 ps and then approaches an asymp-
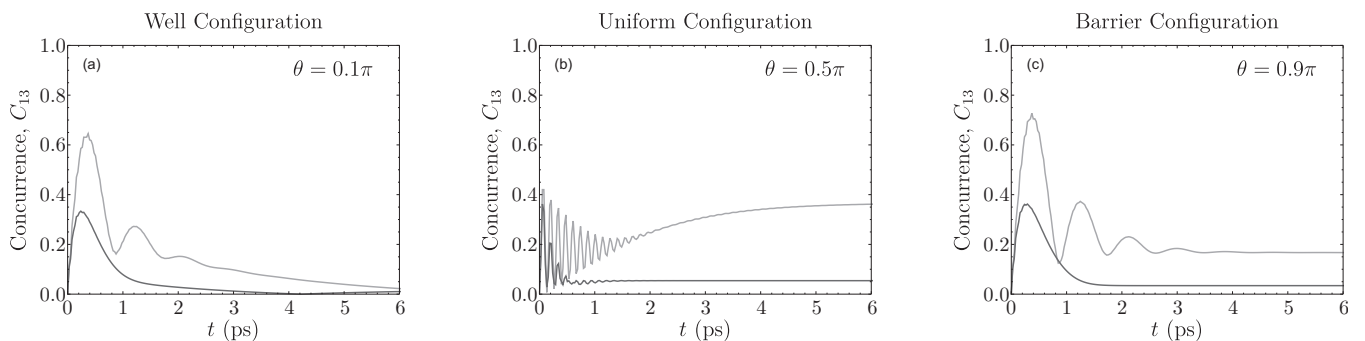
FIG. 6. Plots of the numerical results for the concurrence C_{13} for $\theta = 0.1\pi, 0.5\pi, 0.9\pi$ with bath temperatures of $T = 77$ K (light gray line) and $T = 300$ K (dark gray line).
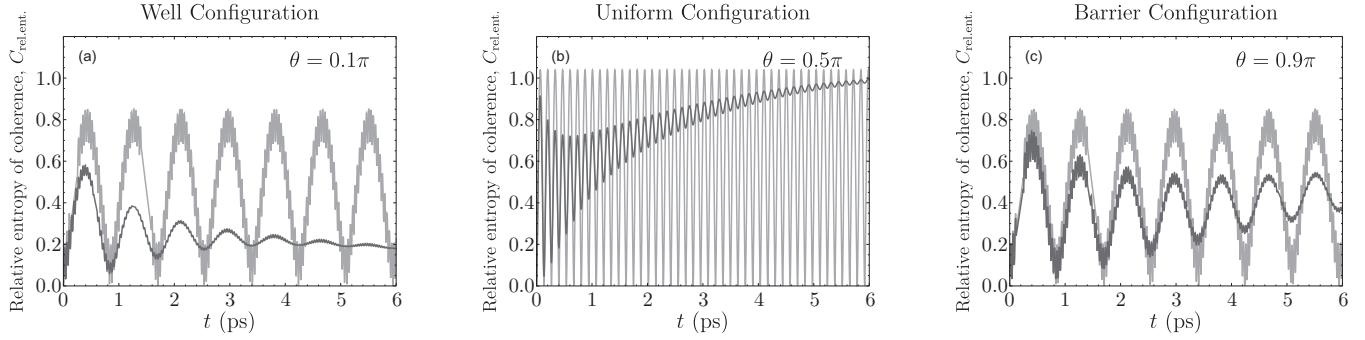
FIG. 7. Plots of the analytic results for the relative entropy of coherence $C_{\text{rel.ent.}}$ for $\theta = 0.1\pi, 0.5\pi, 0.9\pi$ in the absence of a bath (light gray line) and in the presence of a zero-temperature bath (dark gray line).

totic value of 0.02 at 22 ps. The details of this calculation are given in Sec. B 2. At 300 K, C_{13} goes to zero in 4.2 ps and then approaches an asymptotic value of 0.02 at 16.4 ps.

In the barrier configuration, C_{13} consists of damped oscillations with a frequency of 0.5 THz at 77 K, while at 300 K, damping with no appreciable oscillations is observed. At 77 K, the oscillations decay to 1% of their original value in 5.5 ps, approaching an asymptotic value of 0.17. At 300 K, C_{13} approaches an asymptotic value of 0.03 in 1.9 ps.

In the uniform configuration, C_{13} consists of damped oscillations with a frequency of 7.4 THz at 77 K and of 6.9 THz at 300 K. At 77 K, C_{13} approaches an asymptotic value of 0.37 in 7.4 ps, while at 300 K, C_{13} approaches an asymptotic value of 0.05 in 2.9 ps.

E. Relative entropy of coherence for a trimer with no bath and with a thermal bath at absolute zero

Figure 7 shows plots of the analytically derived solution for $C_{\text{rel.ent.}}$ given in Eq. (33), with $\kappa = 0$, $J = 87.7\,\text{cm}^{-1}$, and $\omega_0 = 12\,000\,\text{cm}^{-1}$, and the solution for $C_{\text{rel.ent.}}$ with $\kappa = 0.1$, $J = 87.7\,\text{cm}^{-1}$, and $\omega_0 = 12\,000\,\text{cm}^{-1}$ for an initial state $|egg\rangle$.

From Fig. 7, it is observed that $C_{\text{rel.ent.}}$ is the same for the well and barrier configurations in the absence of a bath, oscillating between 0 and 0.85 with a frequency of 0.59 THz. For the uniform configuration, $C_{\text{rel.ent.}}$ oscillates between 0 and 1.05 with a frequency of 7.43 THz. It is therefore observed that the well and barrier configurations reduce both the os-

cillation frequency and amplitude of $C_{\text{rel.ent.}}$ compared to the uniform configuration.

For the trimer in the presence of a bath at $T = 0\,\text{K}$ (with $\kappa = 0.1$), $C_{\text{rel.ent.}}$ displays different temporal profiles for the well and barrier configurations, as seen in Fig. 7. For the well configuration, $C_{\text{rel.ent.}}$ exhibits damped oscillations with a frequency of 0.59 THz, which approach an asymptotic value of 0.13 in 30 ps. In the barrier configuration, $C_{\text{rel.ent.}}$ exhibits damped oscillations with a frequency of 0.59 THz, with a steady increase in the values of the minima, approaching an asymptotic value of 0.79 in 30 ps. For the uniform configuration, $C_{\text{rel.ent.}}$ exhibits damped oscillations with a frequency of 3.72 THz, with a steady increase in the values of the minima, approaching an asymptotic value of 1.04 in 9 ps.

F. Relative entropy of coherence for a trimer in a thermal bath at $T = 77\,\text{K}$ and $T = 300\,\text{K}$

Figure 8 shows plots of the numerically derived solutions for $C_{\text{rel.ent.}}$ in the presence of the bath at temperatures $T = 77\,\text{K}$ and $T = 300\,\text{K}$. The results are shown for $\kappa = 0.1$, $J = 87.7\,\text{cm}^{-1}$, and $\omega_0 = 12\,000\,\text{cm}^{-1}$, using the same numerical methods as in Sec. IV B.

In the well configuration, $C_{\text{rel.ent.}}$ consists of damped oscillations with a frequency of 0.60 THz at 77 K, while at 300 K, damping with no appreciable oscillations is observed. At 77 K, $C_{\text{rel.ent.}}$ approaches an asymptotic value of 0.13 in 36 ps, while at 300 K, $C_{\text{rel.ent.}}$ goes to zero in 1.9 ps and then approaches an asymptotic value of 0.08 at 22 ps. In the barrier configuration, $C_{\text{rel.ent.}}$ consists of damped oscillations with a
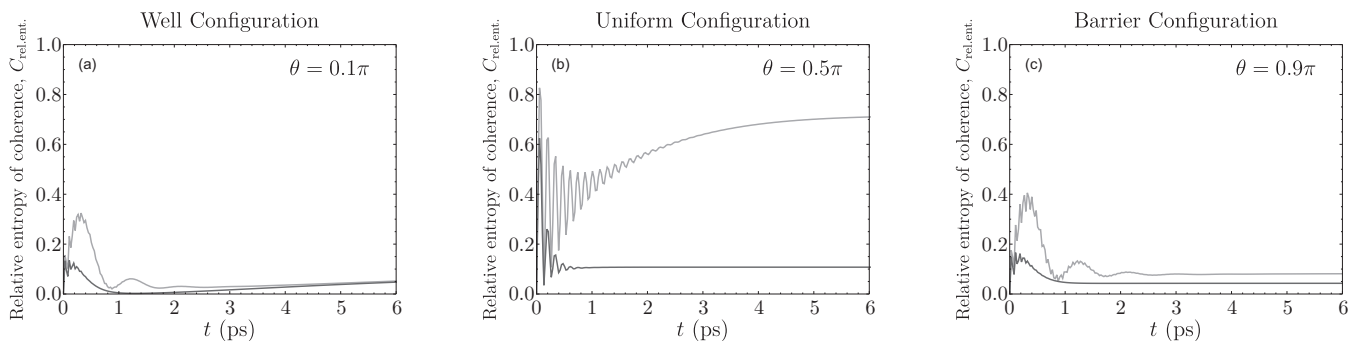
FIG. 8. Plots of the numerical results for the relative entropy of coherence $C_{\text{rel.ent.}}$ for $\theta = 0.1\pi, 0.5\pi, 0.9\pi$ with bath temperatures of $T = 77\,\text{K}$ (light gray line) and $T = 300\,\text{K}$ (dark gray line).
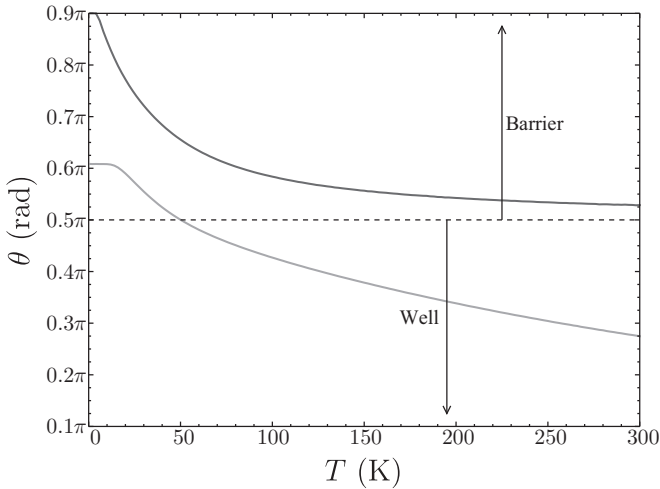
FIG. 9. Plot of mixing angle θ for maximum steady-state concurrence (light gray line) and maximum steady-state relative entropy of coherence (dark gray line) against temperature T.

frequency of 0.51 THz at 77 K, while at 300 K, damping with no appreciable oscillations is observed. At 77 K, the oscillations decay to 1% of their original value in 2.7 ps, approaching an asymptotic value of 0.08 in 5.5 ps, while at 300 K, $C_{\text{rel.ent.}}$ approaches an asymptotic value of 0.04 in 1.4 ps. In the uniform configuration, $C_{\text{rel.ent.}}$ consists of damped oscillations with a frequency of 7.4 THz at 77 and 300 K. At 77 K, $C_{\text{rel.ent.}}$ approaches an asymptotic value of 0.72 in 6.7 ps, while at 300 K, $C_{\text{rel.ent.}}$ approaches an asymptotic value of 0.11 in 0.56 ps.

G. Maximizing steady-state concurrence and relative entropy of coherence

Figure 9 shows the mixing angle θ in the range $0.1\pi \leqslant \theta \leqslant 0.9\pi$ that gives maximum steady-state concurrence $C_{13}^{\max}$ and maximum steady-state relative entropy of coherence $C_{\text{rel.ent.}}^{\max}$ at a given temperature T in the range $0\,\text{K} \leqslant T \leqslant 300\,\text{K}$. At $T = 0\,\text{K}$, $C_{13}^{\max}$ occurs at $\theta = 0.9\pi$, and as temperature increases, the value of θ decreases to $\theta = 0.52\pi$ at 300 K. At $T = 0\,\text{K}$, $C_{\text{rel.ent.}}^{\max}$ occurs at $\theta = 0.61\pi$, and as temperature increases, the value of θ decreases to $\theta = 0.28\pi$ at 300 K.

V. CONCLUSION

In this paper, the authors examined the dynamics of the excitation probabilities, concurrence, and relative entropy of coherence of a trimer in the absence of a bath and in the presence of a thermal bath at $T = 0\,\text{K}$, $T = 77\,\text{K}$, and $T = 300\,\text{K}$. It was found that in the absence of a thermal bath, in both the barrier and well configurations, P_1 and P_3 oscillate with the same frequency, with P_2 being negligible. However, the uniform configuration gave a higher oscillation frequency for P_1 and P_3 compared to well and barrier configurations, with P_2 oscillating at twice the frequency of P_1 and P_3.

For each configuration, it was found that the concurrence and relative entropy of coherence oscillate in phase with each other. This shows a collapse and revival effect of these two quantities in each configuration. In the well and barrier configurations, the maxima occur at points where $P_1 = P_3 \approx 0.5$,

which correspond to near maximally entangled states of the form $\psi_{\pm}^{(1)} = \frac{1}{\sqrt{2}}|egg\rangle \pm \frac{i}{\sqrt{2}}|gge\rangle$ and a great degree of coherent transfer between the first and third TLSs, with negligible excitation transfer to the second TLS. The quantum states of successive maxima alternate between $\psi_+^{(1)}$ and $\psi_-^{(1)}$. In the uniform configuration, the maxima occur at points where $P_1 = P_3 \approx 0.25$ and $P_2 \approx 0.5$, which correspond to an entangled quantum state of the form $\psi_{\pm}^{(2)} = \frac{1}{2}|egg\rangle \pm \frac{i}{\sqrt{2}}|geg\rangle - \frac{1}{2}|gge\rangle$, with a high degree of coherent transfer among the three TLSs. The quantum states of successive maxima alternate between $\psi_+^{(2)}$ and $\psi_-^{(2)}$.

In the presence of a bath at $T = 0\,\text{K}$, P_1 and P_3 oscillate with the same frequency in both the barrier and well configurations but also experience oscillatory damping. The well configuration traps the excitation on the second TLS, while the barrier configuration excludes the excitation from the second TLS, causing the excitation to hop back and forth between the first and third TLSs until steady state is reached. In the uniform configuration, P_1 and P_3 decay more slowly than P_2 and oscillate at twice the amplitude and half the frequency of P_2.

The concurrence and relative entropy of coherence in the well, barrier, and uniform configurations oscillate at the same frequency but also experience oscillatory damping. In the well configuration, the steady state of C_{13} and $C_{\text{rel.ent.}}$ corresponds to an unentangled pure state, $\psi^{(3)} = |geg\rangle$, with localization of the excitation on the second TLS. In the barrier configuration, the steady state of C_{13} and $C_{\text{rel.ent.}}$ corresponds to a near maximally entangled state, $\psi^{(4)} = \frac{1}{\sqrt{2}}(|egg\rangle + |gge\rangle)$), with hopping of the excitation between the first and third TLSs. In the uniform configuration, the steady state of C_{13} and $C_{\text{rel.ent.}}$ corresponds to a less entangled (between the first and third TLSs) quantum state, $\psi^{(5)} = \frac{1}{2}|egg\rangle - \frac{1}{\sqrt{2}}|geg\rangle + \frac{1}{2}|gge\rangle$, with a high degree of coherent transfer among the three TLSs.

In the presence of a bath at $T = 77\,\text{K}$ and $T = 300\,\text{K}$, for the well, barrier, and uniform configurations, P_1, P_2, and P_3 all experience strong oscillatory damping, which increases with temperature. Steady-state times for the probabilities, concurrence, and relative entropy of coherence decrease with increasing temperature for all configurations. In the well configuration, based on Boltzmann statistics in the steady state, the ground-state energy E_1 is populated with near-unit probability at $T = 77\,\text{K}$ and $T = 300\,\text{K}$, with $|geg\rangle$ being the most probable basis state since $\theta = 0.1\pi$. In the barrier configuration, the ground-state energy E_1 is nearly degenerate with E_2, and these are populated with probabilities of 0.59 and 0.41, respectively, at $T = 77\,\text{K}$ and 0.51 and 0.49, respectively, at $T = 300\,\text{K}$, with $|egg\rangle$ and $|gge\rangle$ being the most probable basis states since $\theta = 0.9\pi$. In the uniform configuration, the energy levels E_1, E_2, and E_3 are equally spaced and are populated with probabilities of 0.90, 0.09, and 0.01, respectively, at $T = 77\,\text{K}$ and 0.54, 0.30, and 0.16, respectively, at $T = 300\,\text{K}$. At $T = 77\,\text{K}$, $|geg\rangle$ is twice as probable as $|egg\rangle$ and $|gge\rangle$, whereas at $T = 300\,\text{K}$, all of the basis states are almost equally probable.

The concurrence and relative entropy of coherence in both the well and barrier configurations oscillate at approximately the same frequency but also experience damping. In the well

and barrier configurations, the steady-state values of both these quantities decrease with temperature and are almost negligible at 300 K. However, it should be noted that the uniform configuration is more resistant to changes in concurrence and coherence with increasing temperature than the well and barrier configurations. Therefore, the presence of defects seems to decrease quantum entanglement and coherence as temperature increases.

This trimer model can be generalized and applied in many areas, for example, photosynthetic models, lattice models of trimers, and quantum information science. In photosynthetic models, the quantum decoherence and excitation transfer from donor to acceptor atoms at room temperature can be investigated [6]. In addition, in light-harvesting complexes, the interaction of a trimer with different states of light can also be modeled [20]. In condensed-matter physics, crystalline structures are modeled as several dimer subunits, and this can be extended to crystalline trimer models [21]. Furthermore, electron transfer processes in multiple displaced oscillators coupled to an Ohmic bath in the condensed phase can be in-

vestigated in the nonperturbative regime [22]. Using different couplings and a structured spectral environment, the trimer model can also be used to investigate the energy-transfer mechanism in pigment-protein complexes by utilizing the phonon-antenna mechanism [23]. The real-time dynamics of an exciton propagating through a network based on a quantum circuit [24] can also be investigated. The trimer model can also be used in quantum information to investigate entanglement and decoherence of qubits at finite temperatures. Specifically, the entanglement and decoherence can be investigated when qubits are in different, mixed, or common environments [25] and with static or colored noise [26]. The model can also be used as a design platform for three-qubit quantum logic gates.

APPENDIX A: EIGENVALUES AND EIGENVECTORS OF THE SYSTEM HAMILTONIAN H_s

The eigenvectors $|\lambda_i\rangle$ and eigenvalues E_i ($i = 1, 2, 3$) in the single-excitation manifold of the system Hamiltonian in Eq. (25), where $J_{12} = J_{23} = J$, are

$$|\lambda_1\rangle = \frac{1}{\sqrt{2}} \sin\left(\frac{\theta}{2}\right)|egg\rangle - \cos\left(\frac{\theta}{2}\right)|geg\rangle + \frac{1}{\sqrt{2}} \sin\left(\frac{\theta}{2}\right)|gge\rangle, \tag{A1a}$$

$$E_1 = -\frac{1}{2}\omega_0 - \sqrt{2}J \csc\theta, \tag{A1b}$$

$$|\lambda_2\rangle = -\frac{1}{\sqrt{2}}|egg\rangle + \frac{1}{\sqrt{2}}|gge\rangle, \tag{A1c}$$

$$E_2 = -\frac{1}{2}\omega_0 + \sqrt{2}J \cot\theta, \tag{A1d}$$

$$|\lambda_3\rangle = \frac{1}{\sqrt{2}} \cos\left(\frac{\theta}{2}\right)|egg\rangle + \sin\left(\frac{\theta}{2}\right)|geg\rangle + \frac{1}{\sqrt{2}} \cos\left(\frac{\theta}{2}\right)|gge\rangle, \tag{A1e}$$

$$E_3 = -\frac{1}{2}\omega_0 + \sqrt{2}J \csc\theta, \tag{A1f}$$

where θ is defined in Eq. (24) and $E_1 < E_2 < E_3$ for $0 < \theta < \pi$.

For the case where $J_{12} \neq J_{23}$, the eigenvectors $|\lambda_i'\rangle$ and eigenvalues E_i' are

$$\left|\lambda_1'\right\rangle = \cos\phi \sin\left(\frac{\theta'}{2}\right)|egg\rangle - \cos\left(\frac{\theta'}{2}\right)|geg\rangle + \sin\phi \sin\left(\frac{\theta'}{2}\right)|gge\rangle, \tag{A2a}$$

$$E_1' = -\frac{1}{2}\omega_0 - J_{12} \sec\phi \csc\theta', \tag{A2b}$$

$$\left|\lambda_2'\right\rangle = -\sin\phi|egg\rangle + \cos\phi|gge\rangle, \tag{A2c}$$

$$E_2' = -\frac{1}{2}\omega_0 + J_{12} \sec\phi \cot\theta', \tag{A2d}$$

$$\left|\lambda_3'\right\rangle = \cos\phi \cos\left(\frac{\theta'}{2}\right)|egg\rangle + \sin\left(\frac{\theta'}{2}\right)|geg\rangle + \sin\phi \cos\left(\frac{\theta'}{2}\right)|gge\rangle, \tag{A2e}$$

$$E_3' = -\frac{1}{2}\omega_0 + J_{12} \sec\phi \csc\theta', \tag{A2f}$$

where ϕ, which determines the ratio of the coupling strengths, is defined by

$$\tan\phi = \frac{J_{23}}{J_{12}} \tag{A3}$$

and the mixing angle θ', which represents the inner site's detuning, is given by

$$\tan\theta' = \frac{2\sqrt{J_{12}^2 + J_{23}^2}}{\Delta\omega}. \tag{A4}$$

In this case, $E_1' < E_2' < E_3'$ for $0 < \theta' < \pi$ and $0 < \phi < \frac{\pi}{2}$. It should be noted that Eqs. (A2a)–(A2f) reduce to Eqs. (A1a)–(A1f), respectively, when $J_{12} = J_{23} = J$, $\phi = \frac{\pi}{4}$, and $\theta' = \theta$.

APPENDIX B: NUMERICAL DETERMINATION OF THE PARAMETERS IN F_1 AND F_2

1. Sample calculation of F_1 parameters and decay times

In Sec. III C, Eq. (41) was found to be the best-fit curve to analyze the probabilities at nonzero temperature. For example, the best-fit curve (with an adjusted $R^2 > 0.99$) for P_1 in Fig. 4(a) is given by

$$F_1(t) = 0.49e^{-0.32t} + 0.51e^{-1.19t}\cos(3.34t) + 0.012, \quad \text{(B1)}$$

where the parameters of F_1 are $\alpha_1 = 0.49$, $\gamma_1 = 0.32\,\text{ps}^{-1}$, $\beta_1 = 0.51$, $\lambda_1 = 1.19\,\text{ps}^{-1}$, and $\Omega_1 = 3.34\,\text{rad}\,\text{ps}^{-1}$, and $F_{1,\text{asym}} = 0.012$. To a good approximation, the time for the oscillations to decay is obtained from the exponential part of the second term in Eq. (B1). Specifically, the time for the oscillations to decay to 1% of their initial amplitude is 3.9 ps. To a good approximation, the time taken for $F_1(t)$ to approach the asymptotic value is determined by the first and last terms in Eq. (B1), and the time taken to approach $\pm 1\%$ of the asymptotic value is 26 ps.

2. Sample calculation of F_2 parameters and decay times

In Sec. III C, Eq. (42) was found to be the best-fit curve for the concurrences and relative entropies of coherence at nonzero temperature. For example, the best-fit curve (with an adjusted $R^2 > 0.99$) for C_{13} in Fig. 6(a) is given by

$$
\begin{aligned}
F_2(t) = |0.30e^{-0.31t} - 0.27e^{-2.21t}\cos(0.0018t) \\
+ i[0.00056e^{-0.45t}\sin(0.66t) \\
+ 1.00e^{-1.21t}\sin(3.60t)] - 0.024|, \quad \text{(B2)}
\end{aligned}
$$

where the parameters of F_2 are $\alpha_2 = 0.30$, $\gamma_2 = 0.31\,\text{ps}^{-1}$, $\beta_2 = -0.27$, $\lambda_2 = 2.21\,\text{ps}^{-1}$, $\Omega_2 = 0.0018\,\text{rad}\,\text{ps}^{-1}$, $\alpha' = 0.00056$, $\lambda_2' = 0.45\,\text{ps}^{-1}$, $\Omega_2' = 0.66\,\text{rad}\,\text{ps}^{-1}$, $\beta' = 1.00$, $\lambda_2'' = 1.21\,\text{ps}^{-1}$, $\Omega_2'' = 3.60\,\text{rad}\,\text{ps}^{-1}$, and $F_{2,\text{asym}} = -0.024$. To a good approximation, the time at which $F_2(t) = 0$ is determined by the first and last terms in Eq. (B2) and is found to be 8.1 ps. To a good approximation, the time taken for $F_2(t)$ to approach the asymptotic value is determined by the first and last terms in Eq. (B2), and the time taken to approach $\pm 1\%$ of the asymptotic value is 23 ps.

[1] M. Fox, *Quantum Optics: An Introduction*, Oxford Master Series in Atomic, Optical and Laser Physics (Oxford University Press, Oxford, 2006).

[2] H.-P. Breuer and F. Petruccione, *The Theory of Open Quantum Systems* (Oxford University Press, Oxford, 2003).

[3] S. Blundell, *Magnetism in Condensed Matter* (Oxford University Press, Oxford, 2001).

[4] L. Amico, R. Fazio, A. Osterloh, and V. Vedral, Entanglement in many-body systems, Rev. Mod. Phys. **80**, 517 (2008).

[5] J.-Q. Liao, J.-F. Huang, L.-M. Kuang, and C. P. Sun, Coherent excitation-energy transfer and quantum entanglement in a dimer, Phys. Rev. A **82**, 052109 (2010).

[6] L. A. Pachon and P. Brumer, Physical basis for long-lived electronic coherence in photosynthetic light-harvesting systems, J. Phys. Chem. Lett. **2**, 2728 (2011).

[7] A. Ishizaki and G. R. Fleming, Quantum superpositions in photosynthetic light harvesting: Delocalization and entanglement, New J. Phys. **12**, 055004 (2010).

[8] C. Bengtson and E. Sjoqvist, The role of quantum coherence in dimer and trimer excitation energy transfer, New J. Phys. **19**, 113015 (2017).

[9] Tan Qing-Shou and Kuang Le-Man, Quantum dynamics of entanglement and single excitation transfer in LH1-RC-type trimer, Commun. Theor. Phys. **58**, 359 (2012).

[10] Tan Qing-Shou, Xu Lan, and Kuang Le-Man, Exciton transfer dynamics in a trimer system, Chin. Phys. B **22**, 010304 (2013).

[11] Song Wei, Huang Yi-Sheng, Yang Ming, and Cao Zhuo-Liang, Motion-enhanced quantum entanglement in the dynamics of excitation transfer, Chin. Phys. Lett. **32**, 088701 (2015).

[12] M. B. Plenio and S. F. Huelga, Dephasing-assisted transport: Quantum networks and biomolecules, New J. Phys. **10**, 113019 (2008).

[13] J. Cao and R. J. Silbey, Optimization of exciton trapping in energy transfer processes, J. Phys. Chem. A **113**, 13825 (2009).

[14] I. Kassal and A. Aspuru-Guzik, Environment-assisted quantum transport in ordered systems, New J. Phys. **14**, 053041 (2012).

[15] A. J. Schile and D. T. Limmer, Simulating conical intersection dynamics in the condensed phase with hybrid quantum master equations, J. Chem. Phys. **151**, 014106 (2019).

[16] W. K. Wootters, Entanglement of Formation of an Arbitrary State of Two Qubits, Phys. Rev. Lett. **80**, 2245 (1998).

[17] T. Baumgratz, M. Cramer, and M. B. Plenio, Quantifying Coherence, Phys. Rev. Lett. **113**, 140401 (2014).

[18] M. Ikram, F.-l. Li, and M. S. Zubairy, Disentanglement in a two-qubit system subjected to dissipation environments, Phys. Rev. A **75**, 062336 (2007).

[19] J. Johansson, P. Nation, and F. Nori, QuTiP 2: A Python framework for the dynamics of open quantum systems, Comput. Phys. Commun. **184**, 1234 (2013).

[20] A. G. Dijkstra and A. Beige, Efficient long-distance energy transport in molecular systems through adiabatic passage, J. Chem. Phys. **151**, 034114 (2019).

[21] R. Moessner, S. L. Sondhi, and P. Chandra, Phase diagram of the hexagonal lattice quantum dimer model, Phys. Rev. B **64**, 144416 (2001).

[22] M. Tanaka and Y. Tanimura, Multistate electron transfer dynamics in the condensed phase: Exact calculations from the reduced hierarchy equations of motion approach, J. Chem. Phys. **132**, 214502 (2010).

[23] M. del Rey, A. W. Chin, S. F. Huelga, and M. B. Plenio, Exploiting structured environments for efficient energy transfer: The phonon antenna mechanism, J. Phys. Chem. Lett. **4**, 903 (2013).

[24] A. W. Chin, E. Mangaud, O. Atabek, and M. Desouter-Lecomte, Coherent quantum dynamics launched by incoherent relaxation in a quantum circuit simulator of a light-harvesting complex, Phys. Rev. A **97**, 063823 (2018).

[25] M. Tchoffo, T. K. Lionel, C. Fouokeng, and F. C. Lukong, Quantum correlations dynamics and decoherence of a three-qubit system subject to classical environmental noise, Eur. Phys. J. Plus **131**, 380 (2016).

[26] T. K. Lionel, M. Tchoffo, and F. C. Lukong, Decoherence and protection of entanglement of a system of three qubits driven by a classical Gaussian distributed fluctuating field, Phys. Lett. A **382**, 2805 (2018).